Exciton-phonon coupling in semiconductor quantum dots: Resonant Raman scattering

A. V. Fedorov and A. V. Baranov
S. I. Vavilov State Optical Institute, 199034, St. Petersburg, Russia

K. Inoue
Research Institute for Electronic Science, Hokkaido University, Sapporo, 060, Japan

(Received 20 November 1996)

We study the exciton-phonon coupling in spherical quantum dots (QD's) of cubic semiconductors. Both the Fröhlich and deformation interactions are considered with allowance for all types (LO, T_2O, T_1O, and SO) of optical phonons. The matrix elements of one-phonon transitions between arbitrary exciton states, as well as the selection rules, are determined. Features of different dynamic and optical effects in QD's, e.g., the Jahn-Teller effect, the vibrational resonances, the multiphonon absorption, and the resonant hyper-Raman scattering, are discussed in brief, whereas the resonant Raman scattering (RRS) is studied in more detail. Analytical expressions of the Raman cross section are obtained. Only the confined LO phonons with angular momentum $l=0$ are found to be active in the RRS due to the Fröhlich interaction, while the deformation coupling gives rise to the Raman bands of LO, T_2O, and SO phonons of $l=1$. These conclusions are partly confirmed by the experimental RRS spectra of CuBr nanocrystals in glass, where both the TO and LO phonon bands with comparable intensities are observed. [S0163-1829(97)00136-7]

I. INTRODUCTION

The nature of electron-phonon coupling and its role in the quasiparticle dynamics of semiconductor quantum dots[1–7] (QD's) are still of a great interest. The most extensively studied effect of three-dimensional confinement is the size quantization of quasiparticle energy spectra.[8–10] Another important manifestation of the confinement effect is the renormalization of interactions between all quasiparticles[3,7,10] and between quasiparticles and external fields.[11] Since all three effects are superimposed, their theoretical and experimental elucidation is very difficult. The key problem is the great number of QD's with different sizes and orientations of the crystallographic axes contained in the systems studied. The uncertainty of the QD size distribution causes additional difficulties. That is why the methods of size-selective or resonant spectroscopy are very important in studying the QD systems. Therefore, it is of great interest to the development of the methods of the resonance spectroscopy of a single QD.

Currently, the resonant Raman spectroscopy is one of most powerful tools for studying the quantum confined systems and, in particular, the semiconductor QD's,[3,12–15] where straightforward information about phonon subsystem and electron-phonon coupling in a QD is obtained. Such information is very important for understanding the physics of a confined system and the development of the improved QD model. So far, longitudinal optical (LO) phonons and, to a lesser extent, surface optical (SO) phonons have attracted attention in the studies of QD's in I-IIV, II-IV, and III-V compounds. However, the RRS spectra of CuBr QD's reported in this paper show the transverse optical (TO)- and LO-phonon bands with comparable intensities. This clearly indicates the important role of the deformation exciton-phonon coupling in QD's of cubic semiconductors. Thus a unified description of the Fröhlich and deformation coupling of excitons with all types of optical phonons in nanocrystal LO, T_1O, T_2O, and SO modes[16] is of great interest. We present here a solution of this problem for the spherical QD in a weak confinement regime.[8–10] It is assumed that the QD material is the direct-gap semiconductor with T_d or O_h symmetry and the excitons are located in a potential well with infinitely high walls. The exciton subsystem is described in the effective-mass approximation for the well-known four-band model of the semiconductor,[17] i.e., 12 types of exciton states[18] are considered. For this case, the free exciton and phonon Hamiltonian, as well as the one-phonon and one-photon interaction Hamiltonian, are constructed. Then we derive analytical expressions for the interaction matrix elements and the selection rules for the one-quantum transitions and discuss the size dependence of the exciton-phonon coupling. Our theoretical results are general and can be used for studying the wide range of optical and kinetic effects in QD systems, e.g., the Jahn-Teller effect and vibrational resonance,[7] the exciton-phonon scattering, the multiphonon light absorption, the resonant Raman scattering (RRS), and the resonant hyper-Raman scattering.[19] An analysis of the matrix elements of the exciton-phonon interaction from the RRS standpoint shows that only LO phonons with the angular momentum $l=0$ contribute to the Raman process via the Fröhlich coupling, whereas LO, T_2O, and SO phonons with $l=1$ are involved in the RRS through the deformation coupling. It immediately follows that the TO and LO bands first observed in the CuBr QD resonant Raman spectra correspond to, respectively, T_2O phonons with $l=1$ and LO phonons with $l=0$. Moreover, the shape of the RRS spectra between the T_2O and LO bands indicates the existence of other lines in this region, e.g., those related to the LO and SO phonons with $l=1$. Finally, we find expressions of the cross sections of the RRS from the QD system in the weak confinement regime and on their basis we briefly discuss the RRS excitation profiles in the range of the lowest-energy exciton state. The analysis of the excitation profiles shows

that, even in the case of the Fröhlich interaction, the RRS in QD's cannot be described in terms of the Huang-Rhys parameters since there is not only the significant contribution of different scattering channels to the total amplitude, but also the interference of these channels. Thus our analysis indicates that the observed TO and LO bands correspond to, respectively, the T_2O phonons with the principal quantum number $n=1$ and LO phonons with $n=1$ and $n=2$.

II. THEORY

A. Quantization of the optical vibrational eigenmodes in semiconductor quantum dots

According to the theory of pure phonon modes in finite ionic crystals,[16] there are four types of optical phonons: two types of pure transversal divergence-free modes of frequency ω^T, pure longitudinal curl-free modes of frequency ω^L, and both curl- and divergence-free surface modes of frequency ω^S. Using the direct expressions of optical lattice eigenmodes in semiconductor sphere,[16] we can find the free-phonon Hamiltonian H_0 and the relative displacement of ion pair $\mathbf{u}(\mathbf{r})$,

$$H_0=\sum_{A,\chi}\hbar\omega_\chi^A\left(a_\chi^{A\dagger}a_\chi^A+\frac{1}{2}\right), \tag{1}$$

$$\mathbf{u}(\mathbf{r})=\sum_{A,\chi}B_\chi^A[\mathbf{N}_\chi^A(\mathbf{r})a_\chi^A+\text{H.c.}], \tag{2}$$

where a_χ^A and $a_\chi^{A\dagger}$ are the corresponding annihilation and creation operators and the A and χ indices denote, respectively, the type of mode (T_1, T_2, L, or S) and the set of quantum numbers. For the LO and TO phonons, the subscript χ includes the principal quantum number n, the angular momentum l, and its projection m. For the sake of simplicity, we will also use the composite index $\beta=nl$; then the normalized constants B_χ^L and $B_\chi^{T_i}$ for $i=1$ and 2 are

$$B_{\beta m}^L=\frac{1}{\xi_\beta j_{l+1}(\xi_\beta)}\left(\frac{\hbar}{R\overline{\rho}\,\omega_\beta^L}\right)^{1/2}, \tag{3}$$

$$B_{\beta m}^{T_i}=\frac{1}{j_{l+1}(\xi_\beta)}\left(\frac{\hbar}{l(l+1)R\overline{\rho}\,\omega_\beta^{T_i}}\right)^{1/2} \tag{4}$$

and the vectors $\mathbf{N}_\chi^L(\mathbf{r})$ and $\mathbf{N}_\chi^{T_i}(\mathbf{r})$ are

$$\mathbf{N}_{\beta m}^L(\mathbf{r})=\nabla[\phi_{\beta m}(\mathbf{r})], \tag{5}$$

$$\mathbf{N}_{\beta m}^{T_1}(\mathbf{r})=\text{curl}\left[\frac{\mathbf{r}}{R}\phi_{\beta m}(\mathbf{r})\right], \tag{6}$$

$$\mathbf{N}_{\beta m}^{T_2}(\mathbf{r})=\frac{R}{\xi_\beta}\text{curl}[\mathbf{N}_{\beta m}^{T_1}(\mathbf{r})], \tag{7}$$

$$\phi_{\beta m}(\mathbf{r})=j_l\left(\xi_\beta\frac{r}{R}\right)Y_{lm}(\theta,\varphi). \tag{8}$$

In Eqs. (3)–(8), R is the QD radius, $\xi_\beta=\xi_{nl}$ is the nth root of the spherical Bessel functions of lth order, $j_l(\xi_{nl})=0$, $Y_{lm}(\theta,\varphi)$ is the spherical harmonic, and $\overline{\rho}$ is the reduced ionic mass of the unit cell. It should be noticed that for TO phonons the minimum value of the angular momentum l is 1 and for LO phonons it is 0. As for the eigenfrequencies of LO and TO vibrations, in general, within the framework of the above theory,[16] all the LO phonons have the same frequency ω^L and all the TO phonons have ω^T. To allow for a possible frequency dispersion, we have introduced the phenomenological frequencies ω_β^L, $\omega_\beta^{T_1}$, and $\omega_\beta^{T_2}$ to Eqs. (1)–(4). For the SO phonons the subscript χ denotes both the angular momentum l and its projection m. In this case, similar to the TO phonons, the minimum value of l is 1. The normalized constant B_χ^S and the vector $\mathbf{N}_\chi^S(\mathbf{r})$ are given by

$$B_l^S=\left(\frac{\hbar}{2lR\overline{\rho}\,\omega_l^S}\right)^{1/2}, \tag{9}$$

$$\mathbf{N}_\chi^S(\mathbf{r})=\nabla\left[\left(\frac{r}{R}\right)^l Y_{lm}(\theta,\varphi)\right] \tag{10}$$

and the frequencies of surface modes are presented by

$$\omega_l^S=\omega_T\left[\frac{\varepsilon_0 l+\varepsilon_M(l+1)}{\varepsilon_\infty l+\varepsilon_M(l+1)}\right]^{1/2}, \tag{11}$$

where ε_0 and ε_∞ are the static and the high-frequency dielectric constant and ε_M is that of the surrounding medium.

B. Energy spectra and wave functions of free excitons

To discuss the exciton-phonon interaction in QD's, we should consider the corresponding energy spectra and wave functions of free excitons. For the four-band model of semiconductors, including the doubly degenerate conduction band (c) and twofold degenerate bands of heavy (h_1), light (h_2), and spin-orbit-split (h_3) holes, we should introduce 12 electron-hole pair states,[18] which, using the basis of coupled moments,[20] i.e.,

$$|\widetilde{\varphi}_{1(2)}^{c}\rangle=\left|c,\frac{1}{2},\pm\frac{1}{2}\right\rangle,\quad |\widetilde{\varphi}_{1(2)}^{h_1}\rangle=\left|h_1,\frac{3}{2},\pm\frac{3}{2}\right\rangle,$$

$$|\widetilde{\varphi}_{1(2)}^{h_2}\rangle=\left|h_2,\frac{3}{2},\pm\frac{1}{2}\right\rangle,\quad |\widetilde{\varphi}_{1(2)}^{h_3}\rangle=\left|h_3,\frac{1}{2},\pm\frac{1}{2}\right\rangle, \tag{12}$$

are determined by the expressions

$$\begin{aligned}
&|\widetilde{\psi}_1^1\rangle=|\widetilde{\varphi}_{1,1}^{c,h_1}\rangle,\quad |\widetilde{\psi}_1^2\rangle=|\widetilde{\varphi}_{1,1}^{c,h_2}\rangle,\quad |\widetilde{\psi}_1^3\rangle=|\widetilde{\varphi}_{1,1}^{c,h_3}\rangle,\\
&|\widetilde{\psi}_2^1\rangle=|\widetilde{\varphi}_{1,2}^{c,h_1}\rangle,\quad |\widetilde{\psi}_2^2\rangle=|\widetilde{\varphi}_{1,2}^{c,h_2}\rangle,\quad |\widetilde{\psi}_2^3\rangle=|\widetilde{\varphi}_{1,2}^{c,h_3}\rangle,\\
&|\widetilde{\psi}_3^1\rangle=|\widetilde{\varphi}_{2,1}^{c,h_1}\rangle,\quad |\widetilde{\psi}_3^2\rangle=|\widetilde{\varphi}_{2,1}^{c,h_2}\rangle,\quad |\widetilde{\psi}_3^3\rangle=|\widetilde{\varphi}_{2,1}^{c,h_3}\rangle,\\
&|\widetilde{\psi}_4^1\rangle=|\widetilde{\varphi}_{2,2}^{c,h_1}\rangle,\quad |\widetilde{\psi}_4^2\rangle=|\widetilde{\varphi}_{2,2}^{c,h_2}\rangle,\quad |\widetilde{\psi}_4^3\rangle=|\widetilde{\varphi}_{2,2}^{c,h_3}\rangle,
\end{aligned} \tag{13}$$

where $|\widetilde{\varphi}_{i,j}^{a,b}\rangle=|\widetilde{\varphi}_i^a\rangle|\widetilde{\varphi}_j^b\rangle$. In Eqs. (12), the kets correspond to the Bloch amplitudes and the first and second half-integer indices in the kets are equal to the total momentum (i.e., the sum of angular and spin momenta) and its projection. Assuming that for our basis [Eqs. (12)] the electron and hole

bands are parabolic with the effective masses m_c, m_{h_1}, m_{h_2}, and m_{h_3} and taking into account the Coulomb interaction between quasiparticles of the electron-hole pair, we obtain 12 types of exciton states, which can be naturally classified into three groups. Every group involves four types of exciton states related to one of the three hole bands, so that the energy spectra and the envelope wave functions for every foursome coincide. For the sake of convenience, we call the excitons of corresponding groups heavy, light, or spin-orbit-split excitons. Furthermore, we assume that excitons are located in a spherical potential well with infinitely high walls, so that in the weak confinement regime their energy spectra and wave functions are

$$E_\nu^{(i)}=E_i+\mathrm{Ry}_i\left[-\frac{1}{n^2}+\frac{\mu_i}{M_i}\left(\frac{\xi_{n'l'}}{d_i}\right)^2\right], \tag{14}$$

$$E_{1(2)}=E_g,\quad E_3=E_g+\Delta_{so}, \tag{15}$$

$$|\widetilde{\Psi}^i_{j,\nu}\rangle=\Psi^i_\nu(\mathbf{r},\mathbf{R})|\widetilde{\psi}^{\,i}_j\rangle, \tag{16}$$

where $i=1,2,3$, $j=1,\ldots,4$, the subscript $\nu=\{n',l',m';n,l,m\}$ denotes the set of the principal quantum number, the angular momentum, and its projection for the translational (n',l',m') and relative (n,l,m) motion of the exciton, $M_i=m_c+m_{h_i}$, $\mu_i=m_c m_{h_i}/M_i$, $d_i=R/R_i^{ex}$, $R_i^{ex}=\hbar^2\varepsilon_0/(\mu_i e^2)$, $\mathrm{Ry}_i=\mu_i e^4/2\varepsilon_0^2\hbar^2$ is the exciton Rydberg, E_g and Δ_{so} are the energy gap and spin-orbit splitting in the bulk material, and ξ_{nl} have been defined in Sec. II A. Then, using the composite indices $\beta'=n'l'$ and $\beta=nl$, the envelope wave function in Eq. (16) can be expressed as

$$\Psi^i_\nu(\mathbf{r},\mathbf{R})=\varphi^i_{\beta m}(\mathbf{r})\Psi_{\beta' m'}(\mathbf{R}), \tag{17}$$

where $\Psi_{\beta' m'}(\mathbf{R})$ is the wave function of translational motion[8] and $\varphi^{h_i}_{\beta m}(\mathbf{r})$ is the hydrogenlike wave function[21] of relative motion for the negative energy spectrum

$$\varphi^i_{\beta m}(\mathbf{r})\propto\exp\left(-\frac{r}{nR_i^{ex}}\right). \tag{18}$$

It should be noted that we do not allow for the confinement effect on the exciton relative motion. Using the above definitions and introducing the annihilation and creation operators $b_{k,\nu}$ and $b^\dagger_{k,\nu}$ with the composite index $k=ij$, where i and j label the group of states and the state number in ith group, the free-exciton Hamiltonian can be written as

$$H_{ex}=\sum_{k,\nu}E_\nu^{(i)}\left(b^\dagger_{k,\nu}b_{k,\nu}+\frac{1}{2}\right). \tag{19}$$

In order to calculate the matrix elements of optical transitions, we should also consider the interaction Hamiltonian H_{int} describing the one-photon generation and recombination of excitons in the dipole approximation. We will use the $\mathbf{A}\cdot\mathbf{p}$ representation for the exciton-photon interaction, where $\mathbf{A}=A\mathbf{e}$ is the vector potential of the light wave with the amplitude A and the polarization vector $\mathbf{e}$ and $\mathbf{p}=-i\hbar\nabla$ is the electron momentum operator. Then H_{int} is given by

$$H_{int}=\sum_{k,\nu,\lambda}(L_{k,\nu}b^\dagger_{k,\nu}c_\lambda+\mathrm{H.c.}), \tag{20}$$

where c_λ is the annihilation operator of photon and

$$L_{k,\nu}=i\,\delta_{l',0}\delta_{m',0}\delta_{l,0}\delta_{m,0}\frac{eA}{\hbar c}\frac{(2d_i)^{3/2}P\mathcal{E}_k}{\sqrt{3}\pi n' n^{3/2}}, \tag{21}$$

with

$$\mathcal{E}_{1,j}=\begin{pmatrix}\sqrt{3}e_{+1}\\0\\0\\\sqrt{3}e_{-1}\end{pmatrix},\quad \mathcal{E}_{2,j}=\begin{pmatrix}\sqrt{2}e_0\\e_{-1}\\e_{+1}\\\sqrt{2}e_0\end{pmatrix},\quad \mathcal{E}_{3,j}=\begin{pmatrix}-e_0\\-\sqrt{2}e_{-1}\\\sqrt{2}e_{+1}\\e_0\end{pmatrix}. \tag{22}$$

In the above equations, $e_{\pm1}=\mp(e_x\pm ie_y)/\sqrt{2}$, $e_0=e_z$ are the cyclic covariant components of the polarization vector, $P=\hbar^2\langle S|\partial/\partial z|Z\rangle/m_0$, and m_0 is the free-electron mass. From Eq. (21) it follows that the selection rules for the one-photon generation and recombination of excitons are of the form $l'=l=m'=m=0$.

C. Exciton-phonon interaction in the quantum dot

1. Fröhlich coupling

According to Sec. II A [Eqs. (5) and (10)], only LO and SO phonons induce the electric fields defined by the scalar potentials $\Phi^L(\mathbf{r})$ and $\Phi^S(\mathbf{r})$, respectively:

$$\Phi^L(\mathbf{r})=\sum_{\beta,m}f^L_\beta[\phi_{\beta m}(\mathbf{r})a^L_{\beta m}+\mathrm{H.c.}], \tag{23}$$

$$\Phi^S(\mathbf{r})=\sum_{l,m}f^S_l\left[\left(\frac{r}{R}\right)^l Y_{lm}(\theta,\varphi)a^S_{lm}+\mathrm{H.c.}\right], \tag{24}$$

where

$$f^L_\beta=\frac{1}{\xi_\beta j_{l+1}(\xi_\beta)}\left[\frac{4\pi\hbar\omega^L_\beta}{R}\left(\frac{1}{\varepsilon_\infty}-\frac{1}{\varepsilon_0}\right)\right]^{1/2}, \tag{25}$$

$$f^S_l=\frac{\sqrt{l}\varepsilon_\infty\omega^L_{10}}{\varepsilon_\infty l+\varepsilon_M(l+1)}\left[\frac{2\pi\hbar}{\omega^S_l R}\left(\frac{1}{\varepsilon_\infty}-\frac{1}{\varepsilon_0}\right)\right]^{1/2}. \tag{26}$$

As is well known,[22,23] the potential energy of the exciton in the electric field induced by LO and SO phonons is

$$V^{L(S)}=-e[\Phi^{L(S)}(\mathbf{r}_e)-\Phi^{L(S)}(\mathbf{r}_h)], \tag{27}$$

where $\mathbf{r}_e$ and $\mathbf{r}_h$ are the electron and hole coordinates, and the operator of the Fröhlich coupling can be written as

$$H_F=\sum_{A,k}\sum_{\nu_2,\nu_1,\chi}\left[V_i^{A,\chi}\begin{pmatrix}\nu_2\\\nu_1\end{pmatrix}a^A_\chi b^\dagger_{k,\nu_2}b_{k,\nu_1}+\mathrm{H.c.}\right]. \tag{28}$$

In Eq. (28), as is customary when the Fröhlich coupling is considered, we neglect the interband matrix elements of the potential energy [Eq. (27)]. Because of this, the operator H_F gives rise to transitions between the exciton states belonging to the common type, i.e., it is diagonal for the indices i and j. Extending the results of our recent studies of polar

exciton-LO-phonon coupling[7] to the interaction of excitons with SO phonons and taking into account 12 types of excitons, we obtain the matrix elements of the Fröhlich coupling in the forms

$$V_i^{L,\chi}\begin{pmatrix}\nu_2\\ \nu_1\end{pmatrix}=-\frac{ef_\chi^L}{\sqrt{\pi(2l+1)}}\alpha\begin{pmatrix}l_2',l_2\\ l_1',l_1\end{pmatrix}\delta_{m,m_2-m_1+m_2'-m_1'}$$
$$\times\sum_{p,s=0}^{\infty} i^{p+s-l}(2p+1)(2s+1)I^{\beta;p}_{\beta_2';\beta_1'}J^{\beta;s;i}_{\beta_2;\beta_1}$$
$$\times\mathcal{T}^{l_2',m_2'}_{l_1',m_1';p,m_2'-m_1'}\mathcal{T}^{l,m}_{s,m_2-m_1;p,m_2'-m_1'}$$
$$\times\mathcal{T}^{l_2,m_2}_{l_1,m_1;s,m_2-m_1}, \tag{29}$$

$$V_i^{S,\chi}\begin{pmatrix}\nu_2\\ \nu_1\end{pmatrix}=-\frac{ef_l^S\sqrt{(2l+1)!}}{\sqrt{\pi}}\alpha\begin{pmatrix}l_2',l_2\\ l_1',l_1\end{pmatrix}\delta_{m,m_2-m_1+m_2'-m_1'}$$
$$\times\sum_{p,s=0}^{l=p+s}[(2p)!(2s)!]^{-1/2}I^{p}_{\beta_2';\beta_1'}J^{s;i}_{\beta_2;\beta_1}$$
$$\times C^{l,m}_{p,m_2'-m_1';s,m_2-m_1}$$
$$\times\mathcal{T}^{l_2',m_2'}_{l_1',m_1';p,m_2'-m_1'}\mathcal{T}^{l_2,m_2}_{l_1,m_1;s,m_2-m_1}, \tag{30}$$

where

$$\alpha\begin{pmatrix}l_2',l_2\\ l_1',l_1\end{pmatrix}=\left[\frac{(2l_1+1)(2l_1'+1)}{(2l_2+1)(2l_2'+1)}\right]^{1/2}; \tag{31}$$

the Clebsch-Gordan coefficients[24] $C^{l,m}_{l_2,m_2;l_1,m_1}$ and their combinations

$$\mathcal{T}^{l,m}_{l_2,m_2;l_1,m_1}=C^{l,0}_{l_2,0;l_1,0}C^{l,m}_{l_2,m_2;l_1,m_1}, \tag{32}$$

which determine completely the selection rules for exciton transitions due to the Fröhlich interaction in QD; the constants

$$I^{\beta;p}_{\beta_2';\beta_1'}=\int_0^1 dy\ \ y^2\frac{j_p(y\xi_\beta)j_{l_2'}(y\xi_{\beta_2'})j_{l_1'}(y\xi_{\beta_1'})}{j_{l_2'+1}(\xi_{\beta_2'})j_{l_1'+1}(\xi_{\beta_1'})}, \tag{33}$$

$$I^{p}_{\beta_2';\beta_1'}=\int_0^1 dy\ \ y^{p+2}\frac{j_{l_2'}(y\xi_{\beta_2'})j_{l_1'}(y\xi_{\beta_1'})}{j_{l_2'+1}(\xi_{\beta_2'})j_{l_1'+1}(\xi_{\beta_1'})} \tag{34}$$

are connected with the radial parts of the wave functions $\Psi_{\beta'm'}(\mathbf{R})$ [Sec. II B, Eq. (17)] describing the translational motion of an exciton; the quantities

$$J^{\beta;s;i}_{\beta_2;\beta_1}=R^3\int_0^\eta dx x^2F^i_{\beta_2}(xR)F^i_{\beta_1}(xR)[j_s(\rho_i^h\xi_\beta x)$$
$$-(-1)^s j_s(\rho_i^e\xi_\beta x)], \tag{35}$$

$$J^{s;i}_{\beta_2;\beta_1}=R^3[(\rho_i^h)^s-(-\rho_i^e)^s]\int_0^\eta dx\ \ x^{s+2}F^i_{\beta_2}(xR)F^i_{\beta_1}(xR) \tag{36}$$

are expressed in terms of the radial hydrogenlike wave functions $F^i_\beta(x)$ (Ref. 21) describing the relative motion of the electron and hole; $\rho_i^h=m_{h_i}/M_i$ and $\rho_i^e=m_c/M_i$; and the upper integral limit η is a certain number from 1 to 2. The η uncertainty in Eqs. (35) and (36) arises because the maximum distance between the electron and hole in the QD of radius R lies in the range $R-2R$. In the following estimates we assume that η is equal to 1. From Eqs. (35) and (36) we notice that $J^{\beta;s;i}_{\beta_2;\beta_1}$ and $J^{s;i}_{\beta_2;\beta_1}$ do not vanish for the even values of s only due to the difference between m_c and m_{h_i}. According to the properties of the Clebsch-Gordan coefficients, the even s corresponds to transitions between such exciton states whose angular momenta connected with the relative motion of the electron and hole have the same parity, i.e., $l_1+l_2=2t$ with the integer t. From this it immediately follows that the diagonal part of the Fröhlich coupling does not vanish provided $m_c\neq m_{h_i}$. Due to the availability of the diagonal matrix elements, the exciton-phonon interaction in QD's, to some extent, looks like the electron-vibrational coupling in a molecule or impurity center, so that the notions inherent in these local systems can be used to describe the QD's.

Let us consider in detail the Fröhlich matrix elements controlling some optical processes and the Jahn-Teller effect[7,25] in QD's allowing for the number of low-energy exciton states. From the viewpoint of the RRS, the exciton states with $l_i'=l_i=0$ allowed at the one-photon transitions in the dipole approximation [Eq. (21)] are of great interest and we denote them as $\nu_a(n_i',n_i)=\{n_i',0,0;n_i,0,0\}$. From Eqs. (29)–(36), it is easily obtained that only matrix elements involving LO phonons with $l=0$ do not vanish for such states

$$V_i^{L,\chi}\begin{pmatrix}\nu_a(n_2',n_2)\\ \nu_a(n_1',n_1)\end{pmatrix}=-\frac{ef_\chi^L}{\sqrt{\pi}}\delta_{l,0}\delta_{m,0}I^{n,0;0}_{n_2',0;n_1',0}J^{n,0;0;i}_{n_2,0;n_1,0}. \tag{37}$$

In the case of phonon-assisted absorption and luminescence, as well as the resonant hyper-Raman scattering,[19,26] the matrix elements between $\nu_a(n_i',n_i)$ states and those forbidden at the one-photon transitions [e.g., $\nu_b(\beta_i',m_i')=\{\beta_i',m_i';1,0,0\}$ and $\nu_c(\beta_i,m_i)=\{1,0,0;\beta_i,m_i\}$] play an important role. The characteristic matrix elements of these types are given by

$$V_i^{L,\chi}\begin{pmatrix}\nu_b(\beta',m')\\ \nu_a(1,1)\end{pmatrix}=-\frac{ef_\chi^L}{\sqrt{\pi}}\delta_{l,l'}\delta_{m,m'}I^{\beta;l}_{\beta';1,0}J^{\beta;0;i}_{1,0;1,0},$$

$$V_i^{S,\chi}\begin{pmatrix}\nu_c(\beta_2,m_2)\\ \nu_a(1,1)\end{pmatrix}=-\frac{ef_l^S}{2\sqrt{\pi}}\delta_{l,l_2}\delta_{m,m_2}J^{l;i}_{\beta_2;1,0}. \tag{38}$$

Notice that the Fröhlich coupling between the ν_a and ν_b states does not vanish for the transitions involving only LO phonons, whereas, for the ν_a and ν_c states, transitions involving both LO and SO phonons are possible. These matrix elements also describe two important effects resulting from the vibrational resonance between the initial and final exciton states. Indeed, if the energy gap $E^{(i)}_{\nu_b}-E^{(i)}_{\nu_a}$ or $E^{(i)}_{\nu_c}-E^{(i)}_{\nu_a}$

equals the phonon energy $\hbar\omega^L$ or $\hbar\omega_l^S$, the exciton-phonon interaction is resonant, which will induce renormalization of vibrational frequencies and formation of exciton-vibrational complexes as in the bulk materials.[27] Moreover, a double optical-vibrational resonance at the optical generation of excitons is possible due to the same vibrational resonance.

Finally, let us consider the Fröhlich coupling from the viewpoint of the Jahn-Teller effect, which can be realized in the degenerate exciton states. For simplicity, we restrict ourselves to the threefold states $\nu_b(1,1,m_i')$ and $\nu_c(2,1,m_i)$. From Eqs. (29) and (30) it follows that the exciton in both states can interact with the nondegenerate ($l=0$) and fivefold degenerate ($l=2$) LO phonons. In addition, the exciton in the $\nu_c(2,1,m_i)$ state interacts with the fivefold degenerate ($l=2$) SO phonons. However, it is evident that only the fivefold degenerate phonons are active in the Jahn-Teller effect and corresponding matrix elements are given by

$$V_i^{L,\chi}\begin{pmatrix}\nu_b(1,1,m_2')\\ \nu_b(1,1,m_1')\end{pmatrix}=\frac{ef_{n2}^L}{\sqrt{\pi}}I_{1,1;1,1}^{n,2;2}J_{1,0;1,0}^{n,2;0;i}\hat{W}_m, \tag{39}$$

$$V_i^{S,\chi}\begin{pmatrix}\nu_c(2,1,m_2)\\ \nu_c(2,1,m_1)\end{pmatrix}=\frac{ef_2^S}{2\sqrt{\pi}}J_{2,1;2,1}^{2;i}\hat{W}_m, \tag{40}$$

where

$$\hat{W}_2=\hat{W}_{-2}^{+}=\sqrt{\frac{6}{5}}\begin{pmatrix}0&0&1\\0&0&0\\0&0&0\end{pmatrix},$$

$$\hat{W}_1=-\hat{W}_{-1}^{+}=\sqrt{\frac{3}{5}}\begin{pmatrix}0&-1&0\\0&0&1\\0&0&0\end{pmatrix}, \tag{41}$$

$$\hat{W}_0=\sqrt{\frac{1}{5}}\begin{pmatrix}1&0&0\\0&-2&0\\0&0&1\end{pmatrix}.$$

In Eqs. (41) the subscripts are the projections of the phonon angular momentum and the column (row) numbering from top to bottom (from left to right) corresponds to the projections of the exciton angular momentum related to the translational [Eq. (39)] or relative [Eq. (40)] motion. It can be shown that Eqs. (39) and (40) are reduced to the $T\otimes d$ problem well known in the vibronic interaction theory of the molecular and impurity systems.[28] We emphasize that this dynamic Jahn-Teller effect gives rise to the exciton-phonon complex with the multisheet adiabatic potential.

2. Deformation coupling

As is well known,[17] the deformation potential induced by the optical phonons near the center of the Brillouin zone in cubic semiconductors has only off-diagonal matrix elements involving the heavy (h_1) and light (h_2) hole states. Thus only transitions between the heavy exciton and light exciton states are possible in this case. Taking into account our exciton basis [Eq. (13)] and assuming that the condition $|\rho_1^e-\rho_2^e|\xi_\beta<1$ is satisfied, the operator of the exciton-phonon deformation coupling can be represented as

$$H_D=\sum_{A,k_2,k_1}\sum_{\nu_2,\nu_1,\chi}\left[\left(\hat{\mathbf{S}}_{k_2,k_1}\cdot\mathbf{U}_{i_2,i_1}^{A,\chi}\begin{pmatrix}\nu_2\\ \nu_1\end{pmatrix}\right)\times a_\chi^A b_{k_2,\nu_2}^{\dagger}b_{k_1,\nu_1}+\text{H.c.}\right], \tag{42}$$

where $\hat{\mathbf{S}}$ is the vector 8×8 matrix with the cyclic covariant components

$$[\hat{\mathbf{S}}]_{+1}=-[\hat{\mathbf{S}}]_{-1}^{+}=-\begin{pmatrix}0&0&\sigma_2&0\\0&0&0&\sigma_2\\\sigma_1&0&0&0\\0&\sigma_1&0&0\end{pmatrix}, \tag{43}$$

$$[\hat{\mathbf{S}}]_0=\begin{pmatrix}0&0&\sigma_3&0\\0&0&0&\sigma_3\\\sigma_3&0&0&0\\0&\sigma_3&0&0\end{pmatrix} \tag{44}$$

in terms of the quasiblocks

$$0=\begin{pmatrix}0&0\\0&0\end{pmatrix},\quad \sigma_1=\begin{pmatrix}\sqrt{2}&0\\0&0\end{pmatrix}, \tag{45}$$

$$\sigma_2=\begin{pmatrix}0&0\\0&-\sqrt{2}\end{pmatrix},\quad \sigma_3=\begin{pmatrix}0&i\\-i&0\end{pmatrix} \tag{46}$$

and the row and column numbering in Eqs. (43) and (44) corresponds to the states $|\tilde{\psi}_1^1\rangle,\ldots,|\tilde{\psi}_4^1\rangle,|\tilde{\psi}_1^2\rangle,\ldots,|\tilde{\psi}_4^2\rangle$ defined in Sec. II B [Eq. (13)]. In Eq. (42) the cyclic covariant components of $\mathbf{U}$ vectors are given by

$$\left[\mathbf{U}_{i_2,i_1}^{A,\chi}\begin{pmatrix}\nu_2\\ \nu_1\end{pmatrix}\right]_\lambda=\frac{ip_\chi^A D_0}{\sqrt{\pi(2l+1)}}\alpha\begin{pmatrix}l_2',l_2\\ l_1',l_1\end{pmatrix}\times\delta_{m,m_2-m_1+m_2'-m_1'-\lambda}\times\sum_{p,s=0}^{\infty}i^{p+s-l}(2p+1)(2s+1)\times I_{\beta_2';\beta_1'}^{\beta;p}Z_{\beta_2;\beta_1}^{\beta;s;i_2,i_1}\mathcal{T}_{l_1',m_1';p,m_2'-m_1'}^{l_2',m_2'}\times\mathcal{T}_{l_1,m_1;s,m_2-m_1}^{l_2,m_2}[\mathbf{P}_{s,m_2-m_1;p,m_2'-m_1'}^{l,m;A}]_\lambda, \tag{47}$$

$$\left[\mathbf{U}^{S,\chi}_{i_2,i_1}\begin{pmatrix}\nu_2\\ \nu_1\end{pmatrix}\right]_\lambda = \frac{p_l^S D_0}{\sqrt{\pi(2l+1)}}\alpha\begin{pmatrix}l_2',l_2\\ l_1',l_1\end{pmatrix}\delta_{m,m_2-m_1+m_2'-m_1'-\lambda} \times\sum_{p,s=0}^{l-1}\frac{(2l+1)!!}{(2s+1)!!(2p+1)!!}(2p+1)(2s+1) \times I^p_{\beta_2';\beta_1'}Z^{s;i_2,i_1}_{\beta_2;\beta_1}\mathcal{T}^{l_2',m_2'}_{l_1',m_1';p,m_2'-m_1'} \times\mathcal{T}^{l_2,m_2}_{l_1,m_1;s,m_2-m_1}[\mathbf{P}^{l,m;L}_{s,m_2-m_1;p,m_2'-m_1'}]_\lambda \quad (48)$$

where $A=L,T_1$, and T_2; $\lambda=+1,-1$, and 0; D_0 is the constant of the deformation potential for bulk semiconductor; the combinations of the Clebsch-Gordan coefficients $[\mathbf{P}^{l,m;L}_{l_2,m_2;l_1,m_1}]_\lambda$ are given in Appendix; the $Z^{\beta;s;i_2,i_1}_{\beta_2;\beta_1}$ and $Z^{s;i_2,i_1}_{\beta_2;\beta_1}$ values are determined by the expressions

$$Z^{\beta;s;i_2,i_1}_{\beta_2;\beta_1}=R^3\int_0^\eta dx x^2(-1)^s j_s(\sqrt{\rho_1^e\rho_2^e}\xi_\beta x) \times F^{i_2}_{\beta_2}(xR)F^{i_1}_{\beta_1}(xR), \quad (49)$$

$$Z^{s;i_2,i_1}_{\beta_2;\beta_1}=R^3(-\sqrt{\rho_1^e\rho_2^e})^s\int_0^\eta dx\ \ x^{s+2}F^{i_2}_{\beta_2}(xR)F^{i_1}_{\beta_1}(xR), \quad (50)$$

and the constants p^A_χ are given by

$$p^L_\chi=\frac{\xi_\beta B^L_{\beta m}}{R},\quad p^{A_1}_\chi=\frac{B^{A_1}_{\beta m}}{R}\quad (A_1=T_1,T_2,S). \quad (51)$$

Similarly to the case of the Fröhlich coupling, the selection rules of exciton-phonon transitions via the deformation coupling are completely determined by combinations of the Clebsch-Gordan coefficients [Eqs. 47) and (48)]; however, in contrast to the former case, transitions induced by deformation coupling give rise to the conversion of heavy excitons to the light ones and vice versa.

Let us consider in detail the matrix elements of deformation coupling from the viewpoint of the RRS. As noted in Sec. II C 1, the $\nu_a(n_i',n_i)$ states are of interest for the RRS. These states have the zero angular momentum connected with both the translational and relative motion of excitons. From Eqs. (47) and (48) it follows that only the matrix elements involving threefold-degenerate LO, SO, and T_2O phonons with $l=1$ do not vanish in this case:

$$\left[\mathbf{U}^{A,\chi}_{i_2,i_1}\begin{pmatrix}\nu_a(n_2',n_2)\\ \nu_a(n_1',n_1)\end{pmatrix}\right]_\lambda = U_A\delta_{m,-\lambda}\delta_{l,1}I^{n,1;0}_{n_2',0;n_1',0}Z^{n,1;0;i_2,i_1}_{n_2,0;n_1,0}, \quad (52)$$

$$\left[\mathbf{U}^{S,\chi}_{i_2,i_1}\begin{pmatrix}\nu_a(n_2',n_2)\\ \nu_a(n_1',n_1)\end{pmatrix}\right]_\lambda = U_S\delta_{m,-\lambda}\delta_{l,1}\delta_{n_2',n_1'}Z^{0;i_2,i_1}_{n_2,0;n_1,0}, \quad (53)$$

where $A=L$ or T_2 and

$$U_{A(S)}=\frac{D_0}{\sqrt{3\pi}}\times\begin{cases}p^L_{n1}\\ 2p^{T_2}_{n1}\\ 3p^S_1/2.\end{cases} \quad (54)$$

The peculiarity of coupling with SO phonons is that the principal quantum number of translational motion is conserved at the exciton-phonon transitions ($n_2'=n_1'$) [Eq. (53)]. In principle, the integrals $Z^{n,1;0;i_2,i_1}_{n_2,0;n_1,0}$ and $Z^{0;i_2,i_1}_{n_2,0;n_1,0}$ dependent on the QD radius can be exactly calculated for any particular set of indices. To illustrate this dependence, let us consider the simplest case for $n_2=n_1=1$. Using the notations $d_{12}=d_1+d_2$ and $\varpi_n=\xi_{n1}\sqrt{\rho_1^e\rho_2^e}$, we can represent $Z^{0;i_2,i_1}_{1,0;1,0}$ and $Z^{n,1;0;i_2,i_1}_{1,0;1,0}$ as

$$Z^{0;i_2,i_1}_{1,0;1,0}=\frac{8(d_1d_2)^{3/2}}{(d_{12})^3}\{1-e^{-d_{12}}[1+(1+d_{12})^2]\},$$

$$Z^{n,1;0;i_2,i_1}_{1,0;1,0}=\frac{4(d_1d_2)^{3/2}}{\varpi_n[(d_{12})^2+(\varpi_n)^2]}\Bigg\{\frac{2\varpi_n d_{12}}{(d_{12})^2+(\varpi_n)^2} -e^{-d_{12}}\Bigg[\left(d_{12}+\frac{(d_{12})^2-(\varpi_n)^2}{(d_{12})^2+(\varpi_n)^2}\right)\sin\varpi_n +\left(\varpi_n+\frac{2\varpi_n d_{12}}{(d_{12})^2+(\varpi_n)^2}\right)\cos\varpi_n\Bigg]\Bigg\}. \quad (55)$$

From Eq. (55) it is obvious that the size dependence of exciton-phonon coupling is a complicated function of the QD radius R even in this simplest case. However, the situation is slightly simplified if we can disregard the exponential parts in $Z^{0;i_2,i_1}_{1,0;1,0}$ and $Z^{n,1;0;i_2,i_1}_{1,0;1,0}$,

$$Z^{0;i_2,i_1}_{1,0;1,0}=\frac{8(\mu_1\mu_2)^{3/2}}{(\mu_1+\mu_2)^3}=\text{const}\ (R), \quad (56)$$

$$Z^{n,1;0;i_2,i_1}_{1,0;1,0}=\frac{8d_{12}(d_1d_2)^{3/2}}{[(d_{12})^2+(\varpi_n)^2]^2}. \quad (57)$$

A possibility to neglect the exponential parts is directly connected with the criterion of a weak confinement regime. Indeed, within the framework of the weak confinement approximation,[8] the exponential corrections for the exciton energy spectrum and wave functions are neglected and therefore their account in the matrix elements of exciton-phonon coupling is beyond the scope of this approximation. It should be noted that caution is required in using expressions similar to Eqs. (56) and (57) in the quantitative analysis of experimental data since the criterion of the weak confinement approximation should be verified in each particular case. As follows from Eqs. (56) and (51), the matrix elements of the deformation coupling with SO phonons involved in the RRS are proportional to $R^{-3/2}$. As seen, the matrix elements of the deformation coupling with LO and T_2 O phonons reveal a similar dependence at $R\to\infty$.

3. Size dependence of exciton-phonon coupling

Equations (35), (36), (49), and (50) show that the size dependence of exciton-phonon coupling is determined by the complicated functions of the QD radius R. Explicit forms of these functions depend on the exciton states involved in the matrix elements of corresponding transitions. The forms are particularly controlled by the parameter s, which should satisfy the conditions $|l_2-l_1|<s<l_2+l_1$, where l_i is the angular momentum of exciton relative motion. In principle, the R dependence of matrix elements for each couple of exciton states should be considered in its own right, but within the framework of the exponential approximation (see Sec. II C 2) we can obtain the following general results in the case $R \gg R_i^{ex}$: Matrix elements of the Fröhlich interaction are proportional to $R^{-5/2}$ for LO phonons at $s=0$ and $R^{-s-1/2}$ for LO and SO phonons at $s\neq 0$, whereas matrix elements of the deformation interaction are proportional to $R^{-s-3/2}$ for LO, SO, T_1O, and T_2O phonons. It immediately follows that the size dependences of exciton-phonon matrix elements involved in the different optical processes differ. This fact should be taken into account in the qualitative interpretation of experimental data.

D. Cross section of resonant Raman scattering

The differential cross section of the resonant Raman process for incident light with the frequency Ω_0 and scattered light with the frequency $\Omega_1$is given by

$$\frac{d^2\sigma_{F(D)}}{d\Theta_1 d\Omega_1}=\left(\frac{2eP}{\pi\hbar c}\right)^4\left(\frac{\varepsilon_{\Omega_1}}{\varepsilon_{\Omega_0}}\right)^{1/2}\left(\frac{2\Omega_1}{3\Omega_0}\right)^2\Xi_{F(D)}, \tag{58}$$

where the subscripts F and D denote, respectively, the Fröhlich and deformation exciton-phonon couplings, Θ_1 is the solid angle, and ε_{Ω_1} and ε_{Ω_0} are the dielectric constants at the light frequency. From Sec. II C 1 it follows that, in the dipole approximation, only the LO phonons with the angular momentum $l=0$ are involved in the RRS due to the Fröhlich coupling. Consequently, we can write the factor Ξ_F for Stokes scattering as

$$\begin{aligned}\Xi_F=\frac{e^2}{\pi}\sum_n\ &\delta(\Omega_0-\Omega_1-\omega_{n0}^L)(N_{\omega_{n0}^L}+1)(f_{n0}^L)^2\\ &\times|3(\mathbf{e}_1\cdot\mathbf{e}_0-e_{1z}e_{0z})M_{1,n}+(\mathbf{e}_1\cdot\mathbf{e}_0+3e_{1z}e_{0z})M_{2,n}\\ &+2(\mathbf{e}_1\cdot\mathbf{e}_0)M_{3,n}|^2,\end{aligned} \tag{59}$$

where $\mathbf{e}_0$ and $\mathbf{e}_1$ are the polarization vectors of the incident and scattered light; $N_{\omega_{n0}^L}=[\exp(\hbar\omega_{n0}^L/T)-1]^{-1}$; T is the temperature in energy units; the contributions from the heavy, light, and spin-orbit-split excitons are determined as

$$\begin{aligned}M_{i_1,n}=d_{i_1}^3\sum_{n_1,\ldots,n_2'}&\frac{I^{n,0;0}_{n_2',0;n_1',0}J^{n,0;i_1}_{n_2,0;n_1,0}}{n_1'n_2'(n_1n_2)^{3/2}}\\ &\times(E^{(i_1)}_{\nu_a(n_2',n_2)}-\hbar\Omega_1-i\hbar\gamma^{(i_1)}_{\nu_a(n_2',n_2)})^{-1}\\ &\times(E^{(i_1)}_{\nu_a(n_1',n_1)}-\hbar\Omega_0-i\hbar\gamma^{(i_1)}_{\nu_a(n_1',n_1)})^{-1};\end{aligned} \tag{60}$$

and $\gamma^{(i_1)}_{\nu_a(n_1',n_1)}$ is the inverse lifetime of the corresponding intermediate state. In the case of the deformation coupling (Sec. II C 2), the threefold degenerate LO, T_2O, and SO phonons with $l=1$ are involved to the RRS and hence the factor Ξ_D for Stokes scattering is given by

$$\Xi_D=\Xi_D^L+\Xi_D^{T_2}+\Xi_D^S, \tag{61}$$

where for $A=L$ and T_2

$$\begin{aligned}\Xi_D^A=\frac{D_0^2}{\pi}\sum_n\ &\delta(\Omega_0-\Omega_1-\omega_{n1}^A)(N_{\omega_{n1}^A}+1)U_A^2\{[(e_{1x}e_{0y}\\ &+e_{0x}e_{1y})^2-4e_{1z}^2e_{0z}^2]|M_{A,n}^{\Omega_1,\Omega_0}+M_{A,n}^{\Omega_0,\Omega_1}|^2\\ &+4e_{1z}^2|M_{A,n}^{\Omega_1,\Omega_0}|^2+4e_{0z}^2|M_{A,n}^{\Omega_0,\Omega_1}|^2\\ &+8e_{1z}e_{0z}(\mathbf{e}_1\cdot\mathbf{e}_0)\ \mathrm{Re}(M_{A,n}^{\Omega_1,\Omega_0}[M_{A,n}^{\Omega_0,\Omega_1}]^*)\},\end{aligned} \tag{62}$$

the Ξ_D^S is determined by a similar expression, but without the summation over n, and

$$\begin{aligned}M_{A,n}^{\Omega_1,\Omega_0}=(d_1d_2)^{3/2}&\sum_{n_1,\ldots,n_2'}\frac{I^{n,1;0}_{n_2',0;n_1',0}Z^{n,1;0;2,1}_{n_2,0;n_1,0}}{n_1'n_2'(n_1n_2)^{3/2}}\\ &\times(E^{(2)}_{\nu_a(n_2',n_2)}-\hbar\Omega_1-i\hbar\gamma^{(2)}_{\nu_a(n_2',n_2)})^{-1}\\ &\times(E^{(1)}_{\nu_a(n_1',n_1)}-\hbar\Omega_0-i\hbar\gamma^{(1)}_{\nu_a(n_1',n_1)})^{-1},\end{aligned} \tag{63}$$

$$\begin{aligned}M_S^{\Omega_1,\Omega_0}=(d_1d_2)^{3/2}&\sum_{n_1,n_2,n_1'}\frac{Z^{0;2,1}_{n_2,0;n_1,0}}{(n_1')^2(n_1n_2)^{3/2}}\\ &\times(E^{(2)}_{\nu_a(n_1',n_2)}-\hbar\Omega_1-i\hbar\gamma^{(2)}_{\nu_a(n_1',n_2)})^{-1}\\ &\times(E^{(1)}_{\nu_a(n_1',n_1)}-\hbar\Omega_0-i\hbar\gamma^{(1)}_{\nu_a(n_1',n_1)})^{-1}.\end{aligned} \tag{64}$$

The total spectrum of the RRS is the sum of contributions of the Fröhlich and deformation coupling, i.e., it is described by the quantity $\Xi=\Xi_F+\Xi_D$. The reason is that the RRS via the Fröhlich and deformation couplings involves the different phonons and these channels do not interfere. Obviously, Eqs. (59) and (62) correspond to the RRS from a single QD or system of QD's with the same orientations of the crystallographic axes. In the case of randomly oriented systems, of interest is the RRS cross section averaged over the QD orientations, provided the angle between the polarization vectors $\mathbf{e}_0$ and $\mathbf{e}_1$ is fixed. The averaged cross section is expressed by Eq. (58), where the factors Ξ_F and Ξ_D are replaced with

$$\tilde{\Xi}_F=\frac{e^2}{\pi}\sum_n\ \delta(\Omega_0-\Omega_1-\omega_{n0}^L)(N_{\omega_{n0}^L}+1)(f_{n0}^L)^2$$
$$\times\left(\frac{3}{5}[1+7(\mathbf{e}_1\cdot\mathbf{e}_0)^2]|M_{1,n}+M_{2,n}|^2+4(\mathbf{e}_1\cdot\mathbf{e}_0)^2\right.$$
$$\times\{|M_{3,n}|^2+2\,\mathrm{Re}(M_{1,n}[M_{3,n}]^*+M_{2,n}[M_{3,n}]^*$$
$$\left.-2M_{1,n}[M_{2,n}]^*)\}\right), \tag{65}$$

$$\tilde{\Xi}_D^A=\frac{D_0^2}{3\pi}\sum_n\ \delta(\Omega_0-\Omega_1-\omega_{n1}^A)(N_{\omega_{n1}^A}+1)U_A^2$$
$$\times\left\{8[(\mathbf{e}_1\cdot\mathbf{e}_0)^2-1]\mathrm{Re}(M_{A,n}^{\Omega_1,\Omega_0}[M_{A,n}^{\Omega_0,\Omega_1}]^*)\right.$$
$$\left.+\frac{19-7(\mathbf{e}_1\cdot\mathbf{e}_0)^2}{5}|M_{A,n}^{\Omega_1,\Omega_0}+M_{A,n}^{\Omega_0,\Omega_1}|^2\right\}. \tag{66}$$

Equations (65) and (66) show that, in the general case, the RRS signal depends in a complicated manner on both the incident light parameters and the inherent QD ones. Nevertheless, relatively simple expressions can be written for the RRS involving the lower-energy exciton states. Let us consider particular RRS cross sections. First of all, we shall suggest that the generation energy of the spin-orbit-split excitons is lower than those of the heavy and light excitons. An example of such a situation is the Z_3-exciton band of CuCl QD's. In addition, we assume that the spin-orbit splitting Δ_{so} is sufficiently large to neglect interference of the spin-orbit-split excitons and the heavy (light) ones. Then, if the incident light falls into the Z_3 band, the RRS cross section is determined only by the Fröhlich coupling and the factor $\tilde{\Xi}_F$ can be estimated as

$$\tilde{\Xi}_F=4(\mathbf{e}_1\cdot\mathbf{e}_0)^2\frac{e^2}{\pi}\sum_n\ \delta(\Omega_0-\Omega_1-\omega_{n0}^L)(N_{\omega_{n0}^L}+1)$$
$$\times(f_{n0}^L)^2|M_{3,n}|^2. \tag{67}$$

In the opposite case, when the generation energies of the heavy and light excitons are lower than those of the spin-orbit-split excitons, the situation is more complicated. The $Z_{1,2}$-exciton band of CuBr QD's is a typical example of this situation. If Δ_{so} is sufficiently large to neglect the interference with the spin-orbit-split excitons, the RRS cross section in the case of the resonance with the $Z_{1,2}$ band is determined by both the Fröhlich and deformation couplings. To simplify the problem we suppose that the effective masses m_{h_1} and m_{h_2} are approximately equal. Probably, this approximation is not bad to interpret the RRS spectra obtained by us for CuBr QD's. Substituting $m_{h_1}=m_{h_2}$ in Eqs. (65) and (66), we obtain

$$\tilde{\Xi}_F=\frac{4}{5}[3+(\mathbf{e}_1\cdot\mathbf{e}_0)^2]\frac{e^2}{\pi}\sum_n\ \delta(\Omega_0-\Omega_1-\omega_{n0}^L)(N_{\omega_{n0}^L}+1)$$
$$\times(f_{n0}^L)^2|M_{1,n}|^2, \tag{68}$$

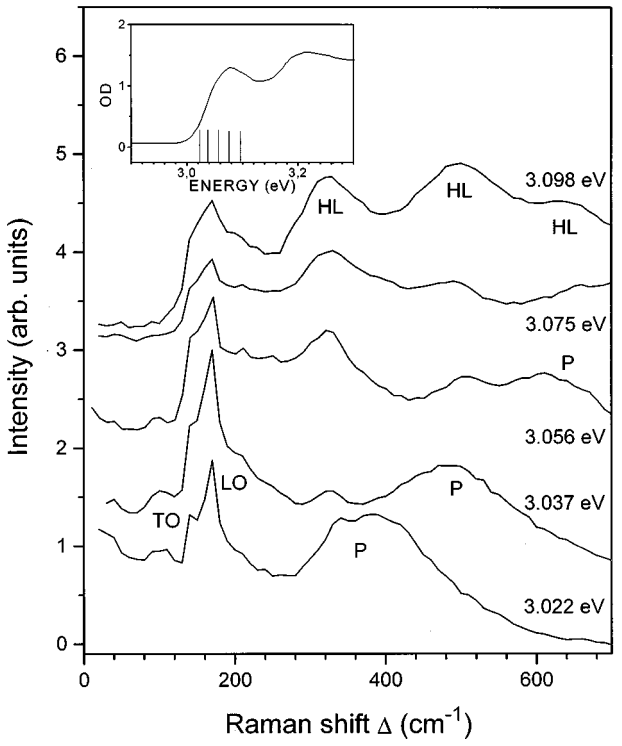

FIG. 1. RRS spectra in the system of CuBr QD's with the average radius 3.2 nm for a number of incident photon energies (as denoted). The frequency origin corresponds to $\Delta=\Omega_0-\Omega_1=0$. The bands denoted as TO, LO, *P*, and HL are assigned to TO phonons, LO phonons, band-edge luminescence, and hot luminescence, respectively. The experimental spectral resolution is 10 cm^{-1}. The inset shows the optical density of the sample; the vertical lines correspond to the incident photon energies. Measurements were made at 2 K.

$$\tilde{\Xi}_D^A=\frac{4}{5}[3+(\mathbf{e}_1\cdot\mathbf{e}_0)^2]\frac{D_0^2}{\pi}\sum_n\ \delta(\Omega_0-\Omega_1-\omega_{n1}^A)$$
$$\times(N_{\omega_{n1}^A}+1)U_A^2|M_{A,n}^{\Omega_1,\Omega_0}|^2, \tag{69}$$

which we use in the analysis of experimental data in the next section.

III. EXPERIMENTS AND RESULTS

The RRS spectra of CuBr QD's at 2 K excited in the region of the $Z_{1,2}$-exciton band were obtained (Fig. 1). We used the same sample, which was examined with the two-photon excitation in Ref. 19, i.e., CuBr nanocrystal in the silicate glass matrix with the average radius $R_0=3.2$ nm. In this case, one can assume that the weak confinement regime is realized for the lower-energy states of the heavy and light excitons since the Bohr radius of the heavy exciton R_1^{ex} in the bulk CuBr is 1.25 nm and the effective masses m_{h_1} and m_{h_2} have close values. The RRS was excited by the pulsed second-harmonic radiation of a tunable Ti-sapphire laser pumped by a *Q*-switch YAG laser (where YAG denotes yttrium aluminum garnet). The average power lower than 3 mW was used with the peak power of 30 W, the pulse width 30 ns, and the repetition rate 3 kHz. Secondary emission was

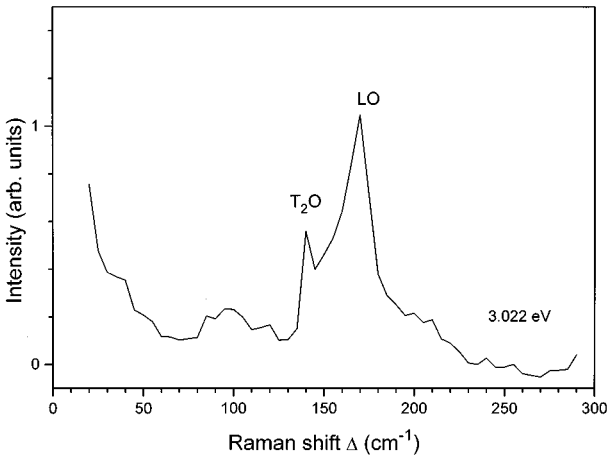

FIG. 2. RRS spectrum for the spectral resolution 5 cm^{-1}. All other parameters are the same as in Fig. 2.

collected in backscattering geometry, dispersed by a U1000 Jobin Ivon double monochromator, and detected by a gated photomultiplier. Absorption of the incident and scattered light was not taken into account. The secondary emission spectra excited by different wavelength are shown in Fig. 1 as a function of the Raman shift as well as the corresponding one-photon absorption spectrum. Several bands are observed in the spectra. Although the spectral resolution of these measurements (10 cm^{-1}) is not sufficient for exact determination of the band positions, it is clearly seen that along with the broad band-edge luminescence and periodic structure with distance between peaks of 165 cm^{-1}, which was assigned in Ref. 19 to the hot luminescence of the coupled exciton-LO-phonon states, two overlapping bands with the Stokes shift of 130–180 cm^{-1} are observed in all spectra. As seen from the RRS spectrum with spectral resolution 5 cm^{-1} (Fig. 2) these bands are narrower than others and have Stokes shift of 140 cm^{-1} and 170 cm^{-1}. It is reasonable to suppose that these bands correspond to the Raman scattering by TO and LO phonons. This assignment is evident because their Stokes shifts are close to those of one-phonon TO and LO bands in the preresonant Raman spectrum of the bulk CuBr at 77 K.[29,30] A detailed analysis of the RRS spectra of CuBr dots with sufficient spectral resolution will be done elsewhere; here it is important to note that the TO and LO phonon bands have comparable intensities in the RRS spectra of CuBr QD's in the weak confinement regime.

According to the theory of the exciton-phonon interaction (Secs. II C 1 and II C 2), only LO phonons with angular momentum $l=0$ and LO, T_2O, and SO phonons with $l=1$ contribute to the RRS via, respectively, the Fröhlich and deformation couplings. Thus we can assign the experimentally observed LO and TO bands to the LO phonons with $l=0$ and T_2O phonons with $l=1$. The shape of the LO band (Fig. 2) allows assumption that there are some additional bands between LO and T_2O ones. So we predict that such bands related to LO and SO phonons with $l=1$ can be observed in the RRS spectra measured with sufficient spectral resolution.

Theoretical analysis of the RRS excitation profiles allows us to identify the exciton states involved in the RRS process in QD's and to find the mode composition of LO and T_2O bands, i.e., the principal quantum numbers n of phonons. Let

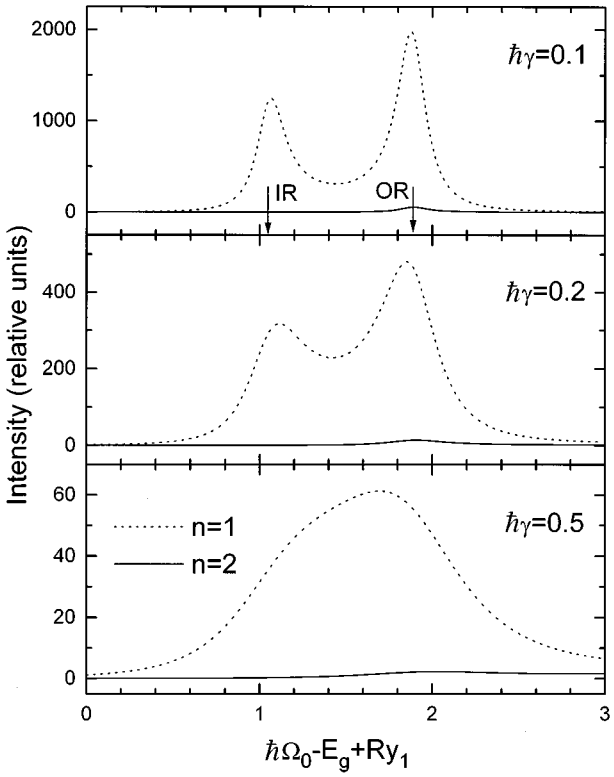

FIG. 3. Exciton profiles of the RRS due to the deformation coupling with T_2O phonons calculated with different inverse lifetime γ of exciton states in the CuBr QD with the radius 3.2 nm. Dotted and solid lines correspond to the cases when $\hbar\Omega_0-\hbar\Omega_1$ equals the energy of phonons with, respectively, $l=1$, $n=1$ and $l=1$, $n=2$. All energy parameters were normalized with respect to the LO-phonon energy. Arrows mark positions of the lowest-energy incoming (IR) and outgoing (OR) resonances.

us assume that the effective masses of the heavy and light holes are equal and, consequently, the corresponding exciton states are degenerated in energy. Then the RRS cross section is given by Eqs. (68) and (69). The composite matrix elements $M_{1,n}$ and $M^{\Omega_1,\Omega_0}_{T_2,n}$ [Eqs. (60) and (63)] consist of the sum of terms having physical meaning of the scattering channels. Every channel has two resonant denominators, which cause the incoming resonance (IR) and outgoing resonance (OR) in the RRS excitation profile with the relative energy shifted by $\Delta_{OI}=E^{(1)}_{\nu_a(n_2',n_2)}+\hbar\omega^A_\beta-E^{(1)}_{\nu_a(n_1',n_1)}$.

The spectral separation of the IR and OR depends on the relationship between $\Delta_{OI}/\hbar$ and the inverse lifetimes of the resonant exciton states $\gamma^{(1)}_{\nu_a(n_2',n_2)}$ and $\gamma^{(1)}_{\nu_a(n_1',n_1)}$. The values γ are, as a rule, unknown and, furthermore, the main mechanisms of the broadening for exciton states are subject to discussion. In our opinion, for QD systems embedded an a dielectric medium, the interaction of QD's with acoustical phonons of the surrounding material is very important for both the broadening of exciton states and the lifetime of optical phonons in QD's. This is caused by the fact that acoustical phonons of dielectric medium, unlike the inner phonons of QD's, have a continuous energy spectrum. However, a detailed discussion of this problem is beyond the scope of our paper and will be done elsewhere. Here we

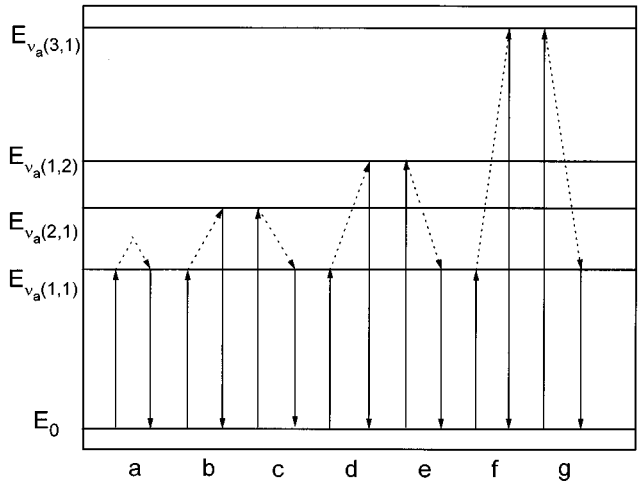

FIG. 4. Diagrams of the RRS channels that significantly contribute to the process amplitudes in the range of the lowest-energy IR and OR. Solid and dotted arrows correspond to, respectively, one-photon and one-phonon transitions. E_0 is the energy of the QD ground state.

assume that the γ's are the phenomenological parameters having the same values for all exciton states. It should be emphasized that the same resonant denominator appears in the expression for a great number of channels; however, not all of them contribute significantly to the magnitudes of the IR or OR. The relative contribution of one channel or another to the specific IR or OR is determined by the matrix elements of exciton-phonon and exciton-photon coupling and the second energy denominator. According to Eqs. (68) and (69), the different RRS channels can interfere constructively or destructively and hence their phase relationships are important for the magnitudes of the IR and OR.

Of most interest in our experimental study are the RRS excitation profiles in the region of the lowest-energy IR and OR related to the exciton state $E_{\nu_a(1,1)}$. Spectral positions of the IR and OR are determined by the energy denominators $E_{\nu_a(1,1)}-\hbar\Omega_0-i\hbar\gamma$ and $E_{\nu_a(1,1)}-\hbar\Omega_0+\hbar\omega_\beta^A-i\hbar\gamma$, respectively. For numerical calculations we used the QD radius of 3.2 nm ($d_1=2.56$) and the following parameters of bulk CuBr: $R_1^{ex}=1.25$ nm, $\mathrm{Ry}_1=105$ meV, $m_e=0.28m_0$, and $m_{h_1}=1.4m_0$.

It was found that the excitation profile of the RRS involving T_2O phonons with $l=1$, $n=1$ (Fig. 3) is formed by three channels whose diagrams a, b, and c are shown in Fig. 4. The magnitudes of the IR and OR are different because of the interference of the channels. The interference is destructive for the IR and constructive for the OR. In the case of a high-γ value, the IR and OR cannot be resolved and as a result we have only one spectral peak. The spectral position of this peak is shifted to the higher-energy side from its position in the absence of interference. At the same time, the magnitudes of excitation profiles for T_2O phonons with $n>1$ are very small compared to that with $n=1$, as seen from Fig. 3, where the excitation profile of the RRS involving T_2O phonons with $l=1$, $n=2$ is also plotted.

The situation is more complicated for the excitation profiles of the RRS involving LO phonons with $l=0$, $n=1$ and

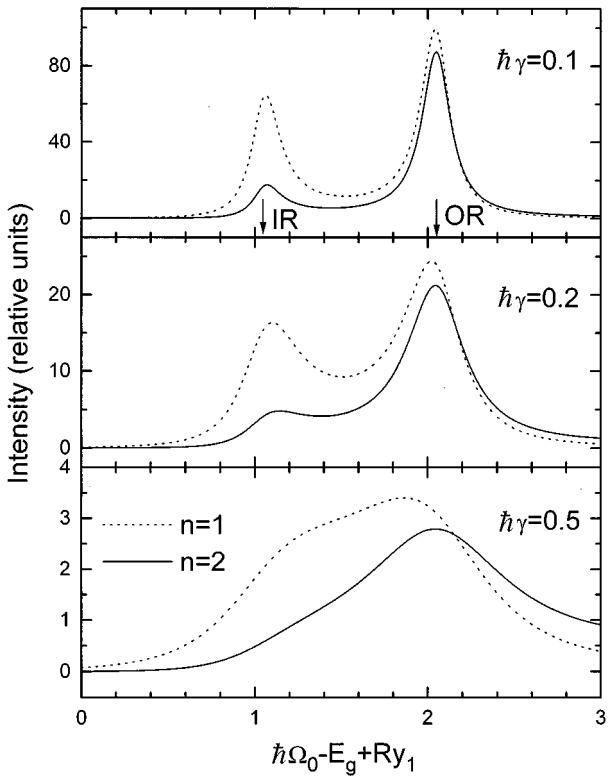

FIG. 5. Calculated exciton profiles of the RRS due to the Fröhlich coupling with LO phonons. Dotted and solid lines correspond to the case when $\hbar\Omega_0-\hbar\Omega_1$ equals the energy of phonons with $l=0$, $n=1$ and $l=0$, $n=2$, respectively. All other parameters are the same as in Fig. 3.

$l=0$, $n=2$. In the former case, the channels a, b, c, d, and e (Fig. 4) significantly contribute to the excitation profile, while in the latter case, instead of the channels d and e, the f and g channels should be taken into account. Since the channels involving the off-diagonal Fröhlich matrix elements (b, c, d, e, f, and g) noticeably contribute to the Raman intensity and strong interference between them exists, the RRS cannot be described in terms of the Huang-Rhys parameters. The excitation profiles corresponding to these cases are shown in Fig. 5, from which we see that the magnitude of the IR for phonons with $n=1$ is much higher that with $n=2$, whereas both magnitudes of the OR are of the same order. This indicates that the excitation profile for phonons with $n=2$ is much more asymmetric than that with $n=1$ and hence, in the case of a high γ, a peak position of the first profile is shifted to the higher-energy side from that of the second profile. As for LO phonons with $l=0$, $n>2$, our calculations show that the excitation profiles of the RRS involving these phonons have very small magnitudes compared to those mentioned above.

As follows from the above discussion, the LO band in the experimental RRS spectra of CuBr dots is likely to be a superposition of the contributions from the LO phonons with $l=0$, $n=1$ and $l=0$, $n=2$, whereas the T_2O band can be assigned to the T_2O phonons with $l=1$, $n=1$.

The size distribution of QD's causes two modifications of the above results. First, the excitation profiles of the RRS are broadened in the ordinary way since the resonant conditions

are realized for any incident photon energy falling into the one-photon absorption band. Therefore, the excitation profiles should look, in a certain sense, like a size-distribution function of QD's. Second, several resonances related to QD's with different radii can be simultaneously realized for fixed incident photon energy. Indeed, if the lowest-energy IR for a QD with the radius R_{IR} exists at the photon energy $\hbar\Omega_0$, then the lowest-energy OR occurs at the same $\hbar\Omega_0$ for a QD with the radius $R_{OR}>R_{IR}$, i.e.,

$$R_{OR}=R_1^{ex}\left[\left(\frac{R_1^{ex}}{R_{IR}}\right)^2-\frac{1}{\pi^2}\frac{M_1}{\mu_1}\frac{\hbar\omega_\beta^A}{Ry_1}\right]^{-1/2}. \tag{70}$$

Similarly, the radii of QD's can be found, for which the IR and OR correspond to other exciton states. The calculated value of R_{OR} is 22 nm for LO phonons and 7.3 nm for T_2O phonons, respectively, if $R_{IR}=R_0=3.2$ nm and therefore the second size effect is negligible in our case for any reasonable size-distribution function of QD's. The discussion of size-distribution effects in more detail will be reasonable only if additional experimental data are obtained, which we will do later.

IV. DISCUSSION

In this paper we developed the theory of the Fröhlich and deformation exciton-phonon couplings involving all the types of optical phonons (LO, T_1O, T_2O, and SO phonons) for spherical QD's of a cubic semiconductor in the weak confinement regime. Analytical expressions of the coupling matrix elements and the selection rules for the one-phonon transitions between arbitrary exciton states were obtained. In addition, the size dependence of the exciton-phonon interaction in the asymptotic limit was discussed.

Let us compare briefly our results and the existing theories. Previously, the Fröhlich interaction between excitons and LO phonons in the weak confinement regime was considered in Refs. 4, 7, and 31. Analytical expressions of the matrix elements of the Fröhlich coupling, calculated in Refs. 7 and 31, are a particular case of the more general equation (29). Since only numerical calculations of the Huang-Rhys parameter were carried out in Ref. 4, a direct comparison of our results with those in Ref. 4 is difficult. However, two points should be emphasized. First, the statement[4] that the nonvanishing coupling constant in the region of the QD sizes, where the Huang-Rhys parameter increases with decreasing QD radius, can be obtained only with allowance for the valence-band mixing is not valid. Indeed, we have shown that the matrix elements of the Fröhlich interaction for transitions between exciton states with the same parity concerning a relative motion and the diagonal matrix elements among them are nonzero due to the Coulomb interaction between the electron and hole and the lack of the wave vector conservation law. In this sense, the QD systems look like the molecular or impurity ones. Furthermore, the diagonal matrix elements of the Fröhlich interaction are nonzero even in the strong confinement regime so long as a spherical potential well with finitely high walls is considered.[32] Second, the numerical calculations of the Huang-Rhys parameter in the range of large QD sizes[4] cast serious doubt on the validity of their results because those calculations show that the Huang-Rhys parameter increases with the increase of QD radius and tends to some nonzero constant for $R\to\infty$. To prove such a size dependence, the Huang-Rhys parameter for bulk semiconductors was estimated in Ref. 4. However, the wave-vector conservation law fulfilled in bulk crystal was not taken into account. Allowance for this law should lead to the zero value of the above constant.

As for the deformation coupling of excitons with optical phonons, we developed the theory of this interaction in the weak confinement regime. Analyzing the deformation coupling, we have assumed that in the cubic semiconductor the exciton-phonon interaction via the deformation potential does not vanish only because of the degeneracy of the valence bands of heavy and light holes. In this case, the electrons and spin-orbit-split holes do not interact with optical phonons and therefore TO and SO phonons are not active in both the RRS and luminescence at excitation of CuCl dots in the Z_3-exciton band. In contrast, the deformation coupling of optical phonons with heavy and light holes leads to the manifestation of the Raman bands corresponding to all type of optical phonons at excitation of CuBr QD's in the $Z_{1,2}$-exciton band.

A comparison of the experimental RRS spectra of CuBr dots with the predictions of the developed theory allows us to assign the observed Raman bands to the LO phonons with $l=0$, $n=1$ and $l=0$, $n=2$ and the T_2O phonons with $l=1$, $n=1$, respectively. A theoretical analysis of the RRS excitation profiles showed that the RRS by a QD system cannot be described in terms of the Huang-Rhys parameters due to the significant contribution of different scattering channels and their interference.

Finally, from our theoretical and experimental results we predicted the possibility of the observation of some additional bands that should be located between LO and T_2O bands. Noteworthy is that such bands correspond to LO and SO phonons with $l=1$

ACKNOWLEDGMENTS

A.V.F. and A.V.B. are grateful to the Russian Basic Research Foundation for financial support of this work through Grants Nos. 96-02-16235a and No. 96-02-16242a.

APPENDIX

The combinations of the Clebsch-Gordan coefficients determining selection rules for exciton-phonon transitions in the case of the deformation coupling are

$$[\mathbf{P}^{l,m;L}_{s,m_s;p,m_p'}]_{+1}=(1+\delta_{m,0})[a(l,-m)\mathcal{T}^{l-1,m+1}_{s,m_s;p,m_p'}-a(l+2,m)\mathcal{T}^{l+1,m+1}_{s,m_s;p,m_p'}], \tag{A1}$$

$$[\mathbf{P}^{l,m;L}_{s,m_s;p,m_p'}]_{-1}=(1-\delta_{m,0})[a(l,m)\mathcal{T}^{l-1,m-1}_{s,m_s;p,m_p'}-a(l+2,-m)\mathcal{T}^{l+1,m-1}_{s,m_s;p,m_p'}], \tag{A2}$$

$$[\mathbf{P}^{l,m;L}_{s,m_s;p,m_p'}]_{0}=b(l,m)\mathcal{T}^{l-1,m}_{s,m_s;p,m_p'}+c(l,m)\mathcal{T}^{l+1,m}_{s,m_s;p,m_p'}, \tag{A3}$$

$$[\mathbf{P}^{l,m;T_1}_{s,m_s;p,m'_p}]_{+1} = -2^{-1/2}(1+\delta_{m,0}) \times \sqrt{(l-m)(l+m+1)}\,\mathcal{T}^{l,m+1}_{s,m_s;p,m'_p}, \tag{A4}$$

$$[\mathbf{P}^{l,m;T_1}_{s,m_s;p,m'_p}]_{-1} = 2^{-1/2}(1-\delta_{m,0}) \times \sqrt{(l+m)(l-m+1)}\,\mathcal{T}^{l,m-1}_{s,m_s;p,m'_p}, \tag{A5}$$

$$[\mathbf{P}^{l,m;T_1}_{s,m_s;p,m'_p}]_{0} = -m\mathcal{T}^{l,m}_{s,m_s;p,m'_p}, \tag{A6}$$

$$[\mathbf{P}^{l,m;T_2}_{s,m_s;p,m'_p}]_{+1} = (1+\delta_{m,0})[(l+1)a(l,-m)\mathcal{T}^{l-1,m+1}_{s,m_s;p,m'_p} + la(l+2,m)\mathcal{T}^{l+1,m+1}_{s,m_s;p,m'_p}], \tag{A7}$$

$$[\mathbf{P}^{l,m;T_2}_{s,m_s;p,m'_p}]_{-1} = (1-\delta_{m,0})[(l+1)a(l,m)\mathcal{T}^{l-1,m-1}_{s,m_s;p,m'_p} + la(l+2,-m)\mathcal{T}^{l+1,m-1}_{s,m_s;p,m'_p}], \tag{A8}$$

$$[\mathbf{P}^{l,m;T_2}_{s,m_s;p,m'_p}]_{0} = (l+1)b(l,m)\mathcal{T}^{l-1,m}_{s,m_s;p,m'_p} - lc(l,m)\mathcal{T}^{l+1,m}_{s,m_s;p,m'_p}, \tag{A9}$$

where

$$a(l,m) = \frac{\sqrt{(l+m)(l-1+m)}}{\sqrt{2}(2l-1)}, \quad b(l,m) = \frac{\sqrt{(l+m)(l-m)}}{2l-1}; \tag{A10}$$

$$c(l,m) = \frac{\sqrt{(l+1+m)(l+1-m)}}{2l+3}. \tag{A11}$$

[1] A. Tamura, K. Higeta, and T. Ichinokawa, J. Phys. C **15**, 4975 (1982); A. Tamura and T. Ichinokawa, *ibid.* **16**, 4779 (1983).

[2] S. Schmitt-Rink, D. A. Miller, and D. S. Chemla, Phys. Rev. B **35**, 8113 (1987).

[3] M. C. Klein, F. Hache, D. Ricard, and C. Flytzanis, Phys. Rev. B **42**, 11 123 (1990).

[4] S. Nomura and T. Kobayashi, Phys. Rev. B **45**, 1305 (1992).

[5] E. Roca, C. Trallero-Giner, and M. Cardona, Phys. Rev. B **49**, 13 704 (1994).

[6] J. C. Marini, B. Stebe, and E. Kartheuser, Phys. Rev. B **50**, 14 302 (1994).

[7] A. V. Fedorov and A. V. Baranov, Zh. Éksp. Teor. Fiz. **110**, 1105 (1996) [JETP **83**, 610 (1996)].

[8] Al. L. Efros and A. L. Efros, Fiz. Tekn. Poluprovodn. **16**, 1209 (1982) [Sov. Phys. Semicond. **16**, 772 (1982)].

[9] E. Hanamura, Phys. Rev. B **37**, 1273 (1988).

[10] Y. Kayanuma, Phys. Rev. B **38**, 9797 (1988).

[11] A. V. Fedorov, A. V. Baranov, and K. Inoue, Phys. Rev. B **54**, 8627 (1996).

[12] A. V. Baranov, Ya. S. Bobovich, and V. I. Petrov, Opt. Spektrosk. **65**, 1066 (1988) [Opt. Spectrosc. **65**, 628 (1988)]; A. P. Alivisatos, T. D. Harris, P. J. Carroll, M. L. Steigerwald, and L. E. Brus, J. Chem. Phys. **90**, 3463 (1989).

[13] A. V. Baranov, Ya. S. Bobovich, and V. I. Petrov, Solid State Commun. **83**, 957 (1992); J. Raman Spectrosc. **24**, 767 (1993).

[14] J. J. Shiang, S. H. Risbud, and A. P. Alivisatos, J. Chem. Phys. **98**, 8432 (1993).

[15] G. Scamarcio, V. Spagnolo, G. Ventruti, M. Lugara, and G. C. Righini, Phys. Rev. B **53**, 10 489 (1996); L. Saviot, B. Champagnon, E. Duval, I. A. Kudriavtsev, and A. I. Ekimov, J. Non-Cryst. Solids **197**, 238 (1996).

[16] R. Englman and R. Ruppin, J. Phys. C **1**, 614 (1968); Rep. Prog. Phys. **33**, 149 (1970).

[17] G. L. Bir and G. E. Pikus, *Symmetry and Strain-Induced Effects in Semiconductors* (Wiley, New York, 1975).

[18] K. Cho, Phys. Rev. B **14**, 4463 (1976).

[19] K. Inoue, A. V. Baranov, and A. Yamanaka, Physica B **219&220**, 508 (1996); K. Inoue, A. Yamanaka, K. Toba, A. V. Baranov, A. A. Onushchenko, and A. V. Fedorov, Phys. Rev. B **54**, 8321 (1996).

[20] H. A. Bethe, *Intermediate Quantum Mechanics* (Benjamin, New York, 1964).

[21] A. Messiah, *Quantum Mechanics* (North-Holland, Amsterdam, 1970).

[22] A. I. Anselm and Yu. A. Firsov, Zh. Eksp. Teor. Fiz. **30**, 719 (1956).

[23] R. S. Knox, *Theory of Excitons* (Academic Press, New York, 1963).

[24] D. A. Varshalovich, A. N. Moskalev, and V. K. Hersonski, *Quantum Theory of Angular Moment* (Nauka, Leningrad, 1975).

[25] *The Dynamical Jahn-Teller Effect in Localized Systems*, edited by Yu. Perlin and M. Wagner (North-Holland, Amsterdam, 1984); A. V. Fedorov, V. A. Kremerman, and A. I. Ryskin, Phys. Rep. **248**, 371 (1994).

[26] A. V. Baranov, K. Inoue, K. Toba, A. Yamanaka, V. I. Petrov, and A. V. Fedorov, Phys. Rev. B **53**, 1721 (1996).

[27] I. B. Levinson and E. I. Rashba, Usp. Fiz. Nauk **111**, 683 (1973) [Sov. Phys. Usp. **16**, 892 (1974)].

[28] M. C. O'Brien, J. Phys. C **4**, 2524 (1971).

[29] Y. Oka, T. Kushida, T. Murahashi, and T. Koda, J. Phys. Soc. Jpn. **36**, 245 (1974).

[30] *Semiconductors*, edited by O. Madelung, M. Schultz, and H. Weiss, Landolt-Börnstein, New Series, Group III, Vol. 17, Pt. a (Springer, Berlin, 1982).

[31] T. Itoh, M. Nishijima, A. I. Ekimov, C. Gourdon, Al. L. Efros, and M. Rosen, Phys. Rev. Lett. **74**, 1645 (1995).

[32] M. P. Chamberlain, C. Trallero-Giner, and M. Cardona, Phys. Rev. B **51**, 1680 (1995).